Karakterisasi Efek *Co-Flow* Jet Sebagai Salah Satu Perangkat kontrol

Characterization of the Co-Flow Jet Effect as One of the Flow Control Devices

James Julian[1]*, Waridho Iskandar[1], Fitri Wahyuni[1], Ferdyanto[2], dan Nely Toding Bunga[3]
[1]Teknik Mesin, Universitas Pembangunan Nasional Veteran Jakarta, Indonesia
[2]Teknik Elektro, Universitas Pembangunan Nasional Veteran Jakarta, Indonesia
[3]Program Studi Teknik Mesin, Fakultas Teknik, Universitas Pancasila, Indonesia

Abstract

The computational study discusses the application of the co-flow jet technique as a fluid flow control device on the NACA 0015 airfoil. The numerical equation used is the RANS equation with the k-ε turbulence model. There are three variations of the mesh proposed in this paper. The first variation is a fine mesh with 100,000 elements. The second variation is a medium mesh with 50,000 elements. Meanwhile, the third variation is coarse mesh with 25,000 elements. Based on the mesh independence test results, the mesh with the lowest error value is the fine mesh. Co-flow jet is proven to control fluid flow on the upper side of NACA 0015. Co-flow jet can also improve the aerodynamic performance of NACA 0015 by increasing Cl and decreasing Cd. The increase in Cl was 114% and the decrease in Cd was 24%. The fluid flow separation on the upper side of the airfoil can also be handled well by the co-flow jet.

Keywords: aerodynamic performance, co-flow jet, flow control, NACA 0015, separation.

Abstrak

Studi komputasional membahas mengenai aplikasi *co-flow jet techinique* sebagai perangkat kontrol aliran fluida pada *airfoil* NACA 0015. Persamaan numerik yang digunakan adalah persamaan RANS dengan model turbulensi $k - \varepsilon$. Terdapat tiga buah variasi *mesh* yang diajukan pada makalah ini. Variasi yang pertama adalah *mesh* halus dengan jumlah elemen 100.000. *Mesh* kedua adalah *mesh* sedang dengan jumlah elemen 50.000. Sementara itu variasi *mesh* ketiga adalah *mesh* kasar dengan jumlah elemen 25.000. Berdasarkan hasil *mesh independence test*, *mesh* yang memiliki nilai kesalahan terendah adalah *mesh* halus. *Co-flow jet* terbukti dapat mengendalikan aliran fluida di sisi atas dari NACA 0015. *Co-flow jet* juga dapat meningkatkan performa aerodinamika NACA 0015 dengan cara meningkatlan C_l dan menurunkan C_d. Peningkatan C_l adalah sebesar 114% dan penurunan C_d sebesar 24%. Pemisahan aliran fluida di sisi atas *airfoil* juga mampu diatasi dengan baik oleh *co-flow jet*.

Kata Kunci: performa aerodinamika, *co-flow jet*, kontrol aliran, NACA 0015, *separasi*.

*Correspondence Author. Phone: -; Handphone: +62 878 8343 9097
email : juliansiregar@gmail.com

1. INTRODUCTION

Fluid flow separation is a phenomenon that can be found in both internal and external fluid flow (Karim and Julian, 2018). In the internal flow, fluid flow separation can be found at the pipe elbow, where fluid flow separation can cause circulating flow. The fluid flow separation in the pipe can cause head losses (Hu *et al.*, 2020). In external flow, the problem of fluid flow separation becomes more complex and can cause substantial losses (Harinaldi *et al.*, 2019, 2020). The fluid flow separation in external flow can be found on the upper side of the airfoil. Airfoil is a cross-sectional shape commonly found on aircraft wings, wind turbine blades, helicopter blades and others. When the airfoil moves with an extreme AoA (angle of attack), the fluid flow cannot follow the shape of the airfoil (Megawanto *et al.*, 2018; Julian, Difitro and Stefan, 2016). The separation of fluid flow on the upper side of the airfoil can cause an increase in the drag force of the airfoil (Harinaldi, Budiarso and Julian, 2016).

From the point of view of the lift force, the separation of the fluid flow can also reduce the lift capability of the airfoil and cause stall conditions (Julian and Karim, 2017). In airfoils, fluid flow separation can occur in various forms. In fluids with a low Reynolds number, fluid flow separation can form a separation bubble. Two types of separation bubbles can be found on the upper side airfoil. The first type of separation bubble is a short separation bubble; the presence of a short bubble does not significantly impact the airfoil. The second type of separation bubble is the long separation bubble. Long separation bubbles can burst at any time on the upper side airfoil. The burst of a long separation bubble can reduce the lift ability of the airfoil. Therefore, at the low Reynolds number, the presence of a separation bubble is avoided (Karim and Julian, 2018; Kosasih, Karim and Julian, 2019). Another type of fluid flow separation on the upper side of the airfoil is peeling off the airfoil's boundary layer. This type of fluid flow separation is often found in medium and high Reynolds numbers (Julian *et al.*, 2018).

Various methods can be used to overcome the fluid flow separation in the airfoil, one of

which is to control the fluid flow around the surface of the airfoil. One of the studies related to flow control around the surface of the airfoil was carried out by Sudhakar and Karthikeyan (Sudhakar and Karthikeyan, 2021). Flow control is carried out by adding tubercles on the airfoil's leading edge. Tubercles are the features that can be found in the humpback whales' fins. The research was carried out experimentally with the object of NACA 4415 at the Reynolds number 120000. The research was explicitly conducted at AoA=18º. Tubercles on the leading edge can reduce fluid flow separation area by 50%. Other research related to flow control was carried out by giving a plasma actuator on the upper side of NACA 4415 (Megawanto *et al.*, 2019). The research was conducted computationally (CFD) on the Reynolds numbers 35,000, 100,000 and 200,000. Based on research conducted by Harinaldi, the plasma actuator can increase the lift force and reduce the drag force of the NACA 4415. The maximum drag force reduction occurs at AoA=15º, where the drag force can be reduced up to 15.01%. Meanwhile, the most significant increase in lift force occurred at AoA=9º, where the increase in lift force occurred at 17.15%.

Using tubercles as a fluid flow control device is only effective at low Reynolds numbers. Therefore, the application of this fluid flow control device is very limited. Meanwhile, the plasma actuator can only delay the fluid flow separation and cannot eliminate the fluid flow separation. Thus, an alternative flow control device is needed to solve the fluid flow separation problem. This research proposes using a co-flow jet as a fluid flow control device. This study aims to apply a co-flow jet as an external fluid flow control device on the upper side of the airfoil and investigate the impact of using a co-flow jet on the NACA 0015 airfoil.

2. METHODOLOGY

The research process in this paper begins with creating the geometry needed for the computational process. The geometric model for this research is NACA 0015; modification of NACA 0015 adjusts to the shape of the co-flow jet and the required domain. The geometries are then

prepared for the meshing process. After the meshing is completed, the research is continued by setting boundary conditions. All of the steps above are part of the pre-processor. After the pre-processor stages are ready, then proceed with doing the solver. Some of the data obtained from the solver process are then tested for the mesh independence test. If the data fails in the mesh independence test stage, it will be repeated in the meshing process. However, if the mesh independence test results successfully. The data can then be collected and grouped for the subsequent analysis. The results of the data analysis can be used to conclude the final result of this research. Overall, the stages of this research can be seen in Figure 1.
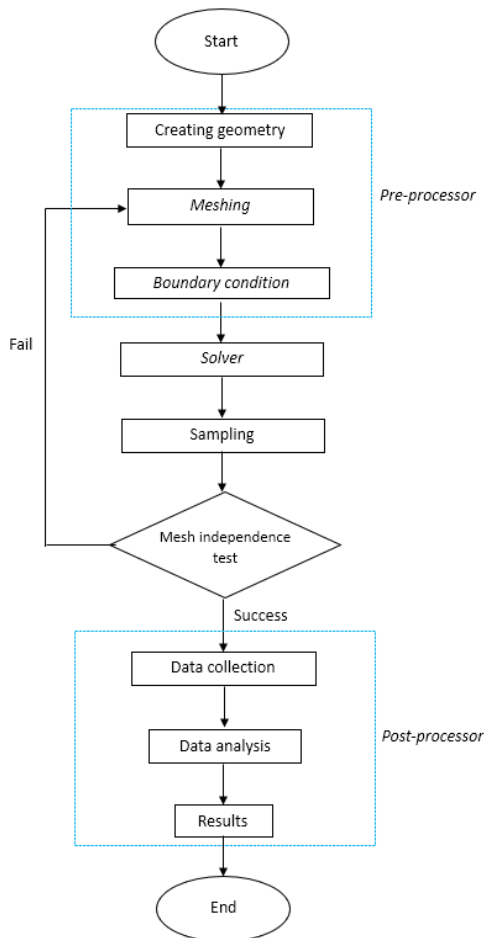

Figure 1. Flowchart of the research

2.1. Co-flow Jet

The co-flow jet is a relatively more modern fluid flow control device. Co-flow jet was first introduced by Zha and Paxton in 2004. Co-flow jet

work by sucking fluid flow from the suction slot and removing the fluid through the injection slot. The injection fluid flowing on the upper side of the airfoil is expected to fill the vacuum when there is a fluid flow separation so that it can delay the stall on the airfoil. The stall is a condition where the airfoil or wing loses lift significantly. The co-flow jet can be seen in Figure 2 (Srinivasan, Ahmed and Sanjana, 2019).
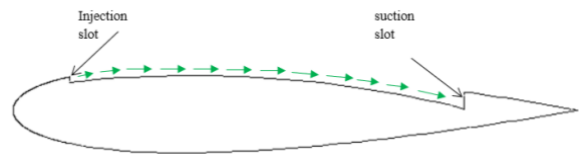

Figure 2. Modified airfoil with co-flow jet

2.2. Geometry

The geometries prepared for computation are the baseline NACA 0015, NACA 0015 with co-flow jets and fluid flow domains. The baseline NACA 0015 and NACA 0015 airfoil with co-flow jets are positioned within the domain. Some of the prepared geometries, along with their dimensions, can be seen in Figure 3. These dimensions are relative to the length of the airfoil chord. The chord length of the NACA 0015 and NACA 0015 airfoils with co-flow jets is 1 meter.
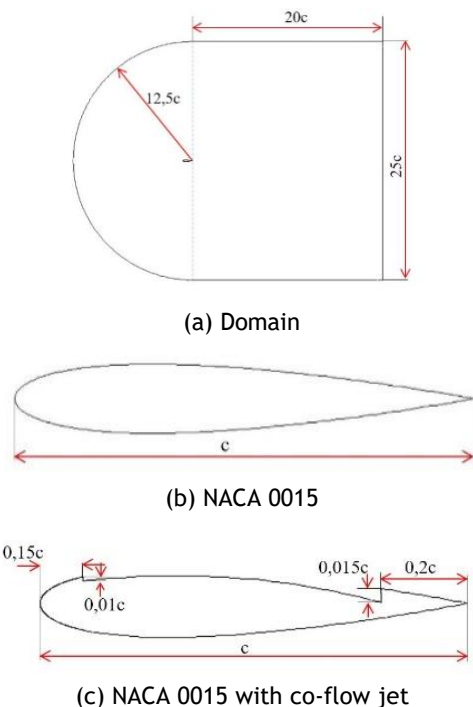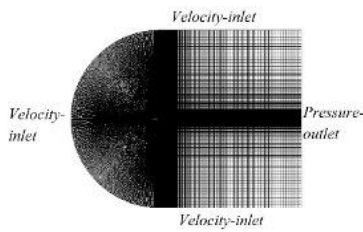

(a) Domain

(b) NACA 0015

(c) NACA 0015 with co-flow jet
Figure 3. Simulation model geometry

2.3. Meshing dan Boundary Condition

In this study, three mesh variations were prepared based on the difference in the number of mesh elements, as shown in Figure 4. The mesh element used was quadrilateral. Boundary conditions on the domain side are velocity-inlet and pressure-outlet. Meanwhile, the boundary condition for the NACA 0015 airfoil is entirely wall (no slip). Furthermore, the boundary condition of the injection slot is the velocity inlet, and the boundary condition for the suction slot is the outlet vent.

(a) Domain
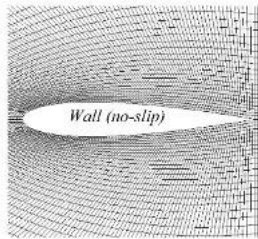
(b) Baseline NACA 0015
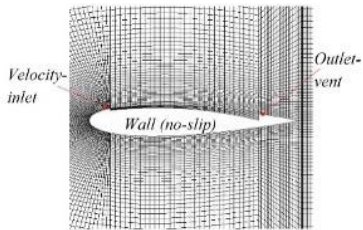
(c) NACA 0015 with co-flow jet
Figure 4. Detail mesh and boundary condition

2.4. Numerical Equations and Turbulence Models

The numerical equation used is the equation for incompressible fluid flow, which is the Reynolds Averaged Navier-Stokes equation. The Reynolds Averaged Navier-Stokes consists of the momentum and mass conservation equations. The turbulence model used is $k - \varepsilon$. k can be used to calculate turbulent kinetic energy. Meanwhile, ε is the dissipation rate to obtain turbulent viscosity estimation. Calculations from numerical equations can be done with equations 1 and 2 (Aftab and Ahmad, 2017). Meanwhile, the mathematical equations for the turbulence model can be seen in equations 3 and 4 (Cable, 2009).

$$\frac{\partial \rho}{\partial t} + \frac{\partial}{\partial x_i}(\rho u_i) = 0 \tag{1}$$

$$\begin{aligned}
&\frac{\partial}{\partial t}(\rho u_i) + \frac{\partial}{\partial x_i}(\rho u_i u_j) = \frac{\partial p}{\partial x_i} \\
&+ \frac{\partial}{\partial x_j}\left[\mu\left(\frac{\partial u_i}{\partial x_j} + \frac{\partial u_j}{\partial x_i} - \frac{2}{3}\delta_{ij}\frac{\partial u_i}{\partial x_i}\right)\right] \\
&+ \frac{\partial}{\partial x_i}\left(-\rho \overline{u_i' u_j'}\right)
\end{aligned} \tag{2}$$

$$\begin{aligned}
\frac{D}{Dt}(\rho k) &= \frac{\partial}{\partial x_j}\left[\left(\mu + \frac{\mu_t}{\sigma_k}\right)\frac{\partial k}{\partial x_j}\right] \\
&+ G_k - \rho\varepsilon
\end{aligned} \tag{3}$$

$$\begin{aligned}
\frac{D}{Dt}(\rho\varepsilon) &= \frac{\partial}{\partial x_j}\left[\left(\mu + \frac{\mu_t}{\sigma_\varepsilon}\right)\frac{\partial \varepsilon}{\partial x_j}\right] \\
&+ C_{e1}\frac{\varepsilon}{k}G_k - \rho C_{\varepsilon 2}\frac{\varepsilon^2}{k}
\end{aligned} \tag{4}$$

2.5. Mesh Independence Test

The mesh independence test is carried out to ensure that the mesh used has a small error value. The first mesh variation has 100,000 elements. It is referred to as fine mesh. The second variation is a medium mesh which has 50,000 elements. Meanwhile, the last variation is a coarse mesh with 25,000 elements. The variation of the mesh can be seen in Figure 5. Mesh independence test can be done by taking a sample of the velocity or pressure of the fluid. The stages of the mesh independence test are carried out sequentially according to the equations below. p is the order of the mesh independence test and r is the ratio between the fine mesh and medium mesh or medium mesh to coarse mesh. GCI_{fine} is a grid convergence index for fine mesh. GCI_{coarse} is a grid convergence index for coarse mesh. $f_{rh=0}$ is the exact value used as a parameter in determining the error value of each mesh. The
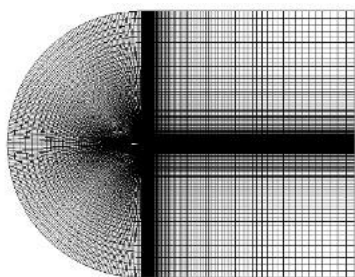
mesh independence test is successful if $\frac{GCI_{fine}}{GCI_{coarse}r^{\bar{\bar{p}}}}$ ≈1. In this study, the mesh independence test is an implementation of a study conducted by Roache (Roache, 1994).
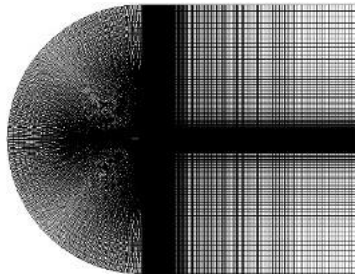
(a) Fine (100000 elements)
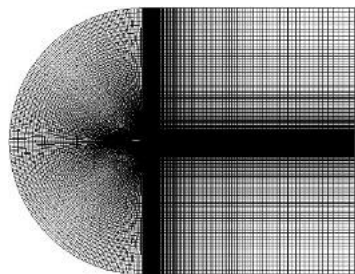
(b) Medium (50000 elements)

(c) Coarse (25000 elements)
Figure 5. Mesh variations

The results of the mesh independence test can be seen in Table 1. Based on the mesh independence test, the mesh variation is in the convergence index range. The number of grids is determined by looking at the lowest error value. Based on Table 1, it can be concluded that the mesh that produces the lowest error is the fine mesh.

3. RESULTS AND DISCUSSION

The Reynolds number chosen in this study is 1.6×10^6, calculated based on the length of the airfoil chord. The velocity of fluid flow injection is twice the free-stream velocity. Aerodynamic data in this study are the lift coefficient (C_l) and drag coefficient (C_d), analyzed in two dimensional. Figure 6 shows the data of C_l through experimental studies and CFD. Experimental data is aerodynamic data of the original NACA 0015 obtained from research conducted by Bertagnolio (Bertagnolio, 2008).

Table 1. Mesh independence test results

Variation	Fine	Medium	Coarse
Velocity	24.427	24.411	24.308
p	2.648		
r	2		
GCI_{fine}	0.016%		
GCI_{coarse}	0.0993%		
$f_{rh=0}$	24.43049		
Results ($\frac{GCI_{fine}}{GCI_{coarse}r^{\bar{\bar{p}}}}$)	1.000668		
Error	0.000127	0.000794	0.004977

This experimental data is used as comparison data. The CFD data in this paper is from the CFD analysis of the baseline NACA 0015 and NACA 0015 with co-flow jets. The C_l data of baseline NACA 0015 shows a trend that resembles the experimental data, especially at AoA≤10º. When AoA>10º, the CFD results predict C_l which slightly deviates from the experimental data. Meanwhile, the CFD and experimental stall were at the same AoA, i.e., AoA=14º. Co-flow jet was proven to increase C_l NACA 0015 by 114%. This increase in C_l is directly affected by fluid flow injection on the airfoil's upper side. The injection of fluid flow can reduce the pressure on the upper side of the airfoil. The lower the pressure on the upper side, the bigger the difference in pressure on the upper and lower sides. Co-flow jet can delay the stall by controlling the fluid flow so that the vacuum area due to recirculation flow on the upper side can be filled. Stall on NACA 0015 with the co-flow jet occurred at AoA=19º. The stall on the NACA 0015 with the co-flow jet does not affect due to

separation flow. The stall is affected by the significant increase of pressure in the injection fluid so that it affects pressure difference across the whole.
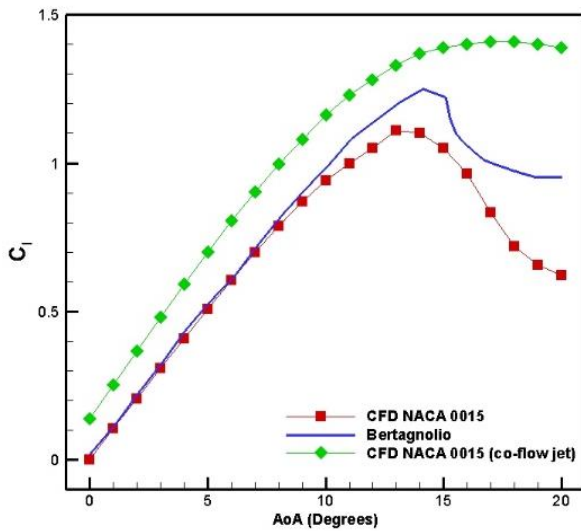

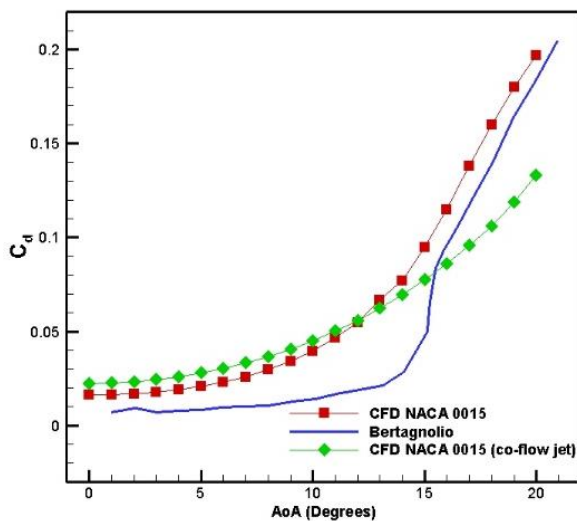**Figure 6.** Graph of C_l against changes in AoA

Figure 7. Graph of C_d against changes in AoA

Besides increasing C_l, co-flow jets can also improve the airfoil's performance by reducing the C_d. The ability to reduce C_d has carried out almost the same principle as increasing C_l. At the extreme AoA, the vacuum in the upper side airfoil is very detrimental, which can cause large C_d. Separation of the fluid flow can increase the value of C_d due to the extreme pressure difference between the fluid flow before interacting with the airfoil and the separated fluid. This extreme pressure difference causes the airfoil to receive a backward thrust. The ability to reduce the C_d of the airfoil can be seen in Figure 7. At AoA>12°, an airfoil with a co-flow jet can produce a smaller C_d compared to the baseline NACA 0015. If the average value is calculated, the decreased C_d equals 24%. Meanwhile, in AoA≤12°, the C_d of the baseline NACA 0015 and NACA 0015 with a co-flow jet were not too different. Compared with experimental results, CFD results in the original NACA 0015 form show a slightly different trend, especially at 13≤AoA≤15°.

Figure 8 shows fluid flow around NACA 0015 with co-flow jet and baseline NACA 0015. Visualization was carried out at AoA 10°, 14° and 19°. Visualization is given in velocity contours and fluid flow streamlines. At AoA=10°, the fluid flow has not yet separated, so the fluid can still cover the entire surface of the airfoil. When the AoA of the airfoil is 14°, a fluid flow separation has formed near the airfoil's trailing edge in the form of a separation bubble. Meanwhile, the fluid flow conditions around the NACA 0015 with the co-flow jet are still not much different compared to AoA=10°. The fluid flow separation in baseline NACA 0015 is more clearly visible when AoA=19°. The fluid flow separation covers almost the entire upper side of baseline NACA 0015. Meanwhile, there is a decrease in velocity near the trailing edge of NACA 0015 with the co-flow jet. However, the fluid flow separation is still not formed.

4. CONCLUSIONS

Research on the application of the co-flow jet as a fluid flow control device was carried out on the NACA 0015 object. Co-flow jet has been proven to control fluid flow to keep flowing on the upper side of the airfoil. Injected fluid flow can improve the aerodynamic performance of NACA 0015. Furthermore, the Co-flow jets can increase the lift force of NACA 0015 and delay stall conditions. In addition, the co-flow jet can reduce the Cd of the airfoil at AoA>12°. Co-flow jet can also overcome fluid flow separation in both the form of bubbles and circulating areas.

(a) NACA 0015 with co-flow jet 10°

(b) baseline NACA 0015 10°

(c) NACA 0015 with co-flow jet 14°

(d) baseline NACA 0015 14°

(e) NACA 0015 with co-flow jet 19°
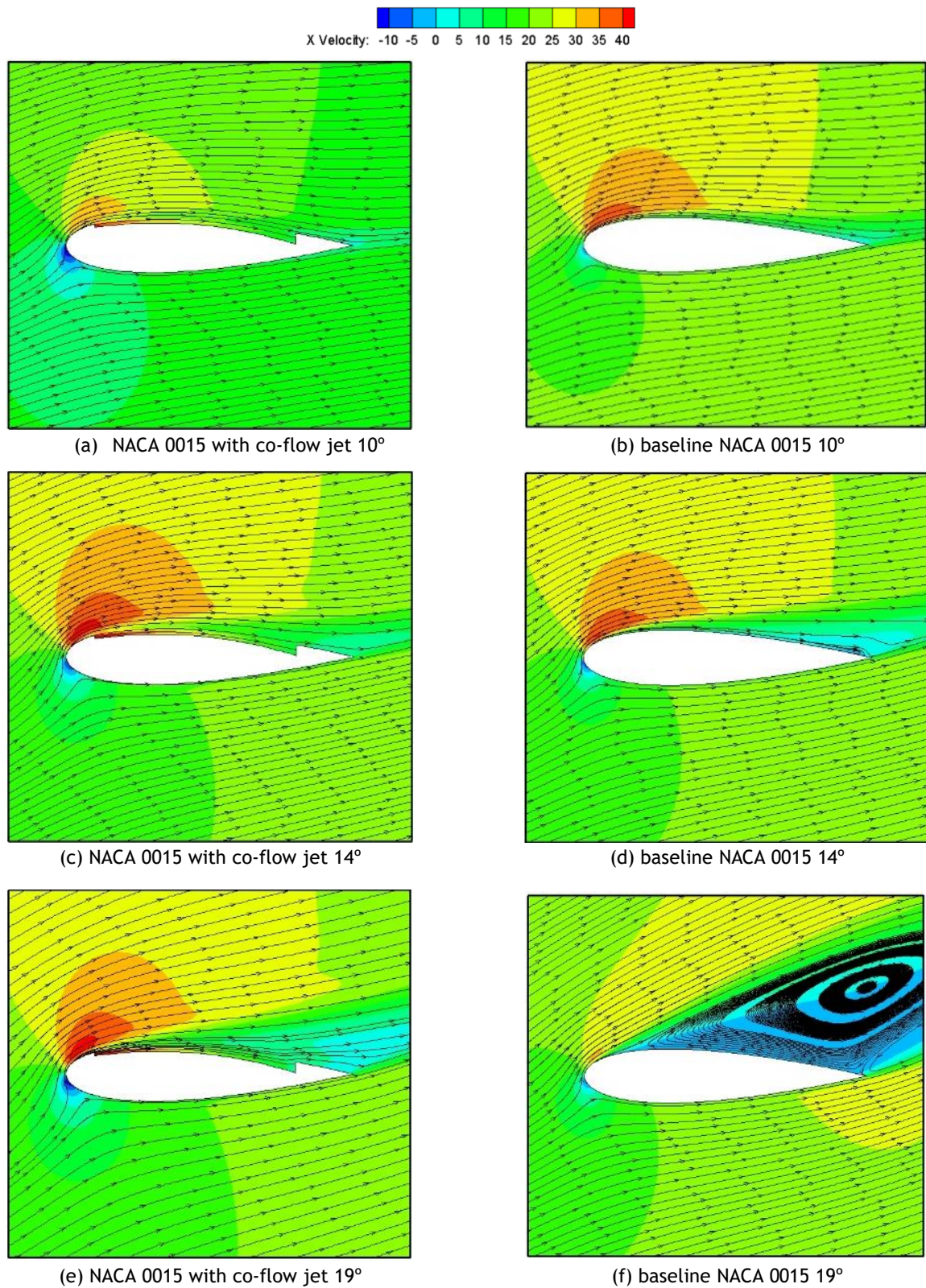
(f) baseline NACA 0015 19°

Figure 8. Velocity contours and fluid flow streamlines.

REFERENCES

Aftab, S.M.A. and Ahmad, K.A. (2017) 'Correction: CFD study on NACA 4415 airfoil implementing spherical and sinusoidal Tubercle Leading Edge', *Plos one*, 12(11), p. e0188792.

Bertagnolio, F. (2008) 'NACA0015 measurements in LM wind tunnel and turbulence generated noise'. Denmark.

Cable, M. (2009) *An evaluation of turbulence models for the numerical study of forced and natural convective flow in Atria*. PhD Thesis. Queen's University.

Harinaldi *et al*. (2019) 'The comparison of an analytical, experimental, and simulation approach for the average induced velocity of a dielectric barrier discharge (DBD)', in *AIP Conference Proceedings*. AIP Publishing LLC, p. 020027.

Harinaldi, Budiarso and Julian, J. (2016) 'The effect of plasma actuator on the depreciation of the aerodynamic drag on box model', in *AIP Conference Proceedings*. AIP Publishing LLC, p. 040004.

Harinaldi, K.M.D. *et al*. (2020) 'Flow control with multi-dbd plasma actuator on a delta wing', *Evergreen*, 7(4), pp. 602–608.

Hu, Q. *et al*. (2020) 'Experimental and numerical investigation on the transport characteristics of particle-fluid mixture in y-shaped elbow', *Journal of Marine Science and Engineering*, 8(9), p. 675.

Julian, J. *et al*. (2018) 'Effect of plasma actuator in boundary layer on flat plate model with turbulent promoter', *Proceedings of the Institution of Mechanical Engineers, Part G: Journal of Aerospace Engineering*, 232(16), pp. 3001–3010.

Julian, J., Difitro, R. and Stefan, P. (2016) 'The effect of plasma actuator placement on drag coefficient reduction of Ahmed body as an aerodynamic model', *International Journal of Technology*, 7(2), pp. 306–313.

Julian, J. and Karim, R.F. (2017) 'Review: Flow control on a squareback model', *International Review of Aerospace Engineering*, 10(4), pp. 230–239.

Karim, R.F. and Julian, J. (2018) 'Drag reduction due to recirculating bubble control using plasma actuator on a squareback model', in *MATEC Web of Conferences*. EDP Sciences, p. 01108.

Kosasih, E.A., Karim, R.F. and Julian, J. (2019) 'Drag reduction by combination of flow control using inlet disturbance body and plasma actuator on cylinder model', *Journal of Mechanical Engineering and Sciences*, 13(1), pp. 4503–4511.

Megawanto, F.C. *et al*. (2018) 'Numerical analysis of plasma actuator for drag reduction and lift enhancement on NACA 4415 airfoil', in *AIP Conference Proceedings*. AIP Publishing LLC, p. 050001.

Megawanto, F.C. *et al*. (2019) 'Flow separation delay on NACA 4415 airfoil using plasma actuator effect', *International Review of Aerospace Engineering*, 12(4), pp. 180–186.

Roache, P.J. (1994) 'Perspective: a method for uniform reporting of grid refinement studies', *J. Fluids Eng.*, 116(3), pp. 405-413.

Srinivasan, S., Ahmed, T. and Sanjana, G.K. (2019) 'Numerical and Experimental Investigation of Co-Flow Jet Technique in Clarky-M18 Aerofoil', in *Proceedings of the Second International Conference on Emerging Trends in Science & Technologies For Engineering Systems (ICETSE-2019)*.

Sudhakar, S. and Karthikeyan, N. (2021) 'Flow Separation Control on a NACA-4415 Airfoil at Low Reynolds Number', in *Proceedings of 16th Asian Congress of Fluid Mechanics*. Springer, pp. 323–334.